JOC The Journal of Organic Chemistry

ARTICLE

pubs.acs.org/joc

Reaction Mechanism and Chemoselectivity of Intermolecular Cycloaddition Reactions between Phenyl-Substituted Cyclopropenone Ketal and Methyl Vinyl Ketone

Yan Qiao[†] and Tian-Shu Chu[*,†,‡]

[†]State Key Laboratory of Molecular Reaction Dynamics, Dalian Institute of Chemical Physics, Chinese Academy of Sciences, Dalian 116023, China

[‡]Institute for Computational Sciences and Engineering, Laboratory of New Fiber Materials and Modern Textile, The Growing Base for State Key Laboratory, Qingdao University, Qingdao, 266071, China

Supporting Information

ABSTRACT: In this paper, the mechanisms of the intermolecular [3 + 2] and [1 + 2] cycloaddition reactions of 1,1/1,3-dipolar π-delocalized singlet vinylcarbenes, which is obtained from cyclopropenone, with an electron-deficient C═O or C═C dipolarophile, to generate five-membered ring products are first disclosed by the density functional theory (DFT). Four reaction pathways, including two concerted [3 + 2] cycloaddition reaction pathways and two stepwise reaction pathways (an initial [1 + 2] cycloaddition and then a rearrangement from the [1 + 2] cycloadducts to the final [3 + 2] cycloadducts), are investigated at the B3LYP/6-31G(d,p) level of theory. The calculated results reveal that, in contrast to the concerted C═O [3 + 2] cycloaddition reaction pathway, which is 7.1 kcal/mol more energetically preferred compared with its stepwise reaction pathway, the C═C dipolarophile favors undergoing [1 + 2] cycloaddition rather than concerted [3 + 2] cycloaddition (difference of 5.3 kcal/mol). The lowest free energy barrier of the C═O concerted [3 + 2] cycloaddition reaction pathway shows that it predominates all other reaction pathways. This observation is consistent with the finding that the C═O [3 + 2] cycloadduct is the main product under experimental conditions. In addition, natural bond orbital second-order perturbation charge analyses are carried out to explain the preferred chemoselectivity of C═O to the C═C dipolarophile and the origins of *cis*-stereoselectivity for C═C [1 + 2] cycloaddition. Solvent effects are further considered at the B3LYP/6-31G(d,p) level in the solvents CH_3CN, DMF, THF, CH_2Cl_2, toluene, and benzene using the PCM model. The results indicate that the relative reaction trends and the main products are insensitive to the polarity of the reaction solvent.

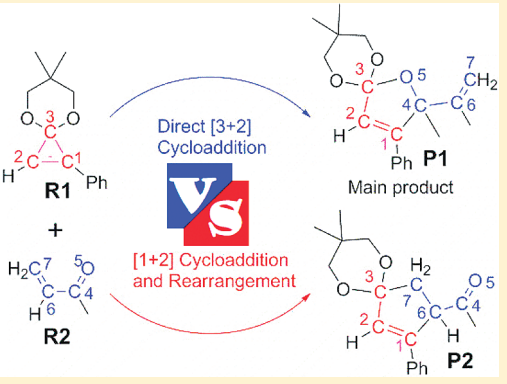

INTRODUCTION

The thermal [3 + 2] cycloaddition reaction between 1,3-dipoles and dipolarophiles complements the Diels−Alder [4 + 2] cycloaddition reaction that is extensively applied in the synthesis of functionalized six-membered rings.[1] This kind of 1,3-dipolar cycloaddition allows the production of various five-membered carbocycles and heterocycles,[2] which can subsequently be used to construct many important natural products. To date, many dipolar and dipolarophile cycloaddition partners have been explored, characterized, and applied in heterocycle synthesis.[3] In contrast, the development and application of simple three-carbon 1,3-dipoles in thermal cycloaddition reactions have not been described very well.[3] However, their potential participation in [3 + 2] cycloaddition reactions for the construction of functionalized cyclopentenes is of special interest since each of the five carbons of the newly formed five-membered ring bears functionalities suitable for additional transformation.[4] In the past, much effort has been devoted to the development and application of three-carbon 1,3-dipoles, including the discoveries by Trost et al. regarding the palladium-promoted asymmetric [3 + 2] cycloaddition of trimethylenemethane,[5] Lu et al.'s three-carbon plus two-carbon addition reaction catalyzed by tertiary phosphines,[6] Boger et al.'s thermal [3 + 2] cycloaddition reaction between 1,1/1,3-dipolar π-delocalized singlet vinylcarbenes obtained from cyclopropenone and an electron-deficient dipolarophile,[1,4,7] as well as many other endeavors.[8] Remarkably, all of these reactions, except Boger et al.'s, successfully proceeded with the aid of catalysts, such as a transition metal, Lewis acids, or tertiary phosphines. Boger et al.'s method is very attractive since it is convenient and free of rigorous experimental conditions.

On the basis of Boger et al.'s experimental results,[4,7b−7d] the reactions are initiated by the formation of 1,1/1,3-dipolar π-delocalized singlet vinylcarbenes, which then react with C═O or C═C dipolarophiles by way of [3 + 2] and [1 + 2] cycloaddition.

Received: December 15, 2010
Published: March 25, 2011

Scheme 1. Four Possible Reaction Pathways of the Title Reaction

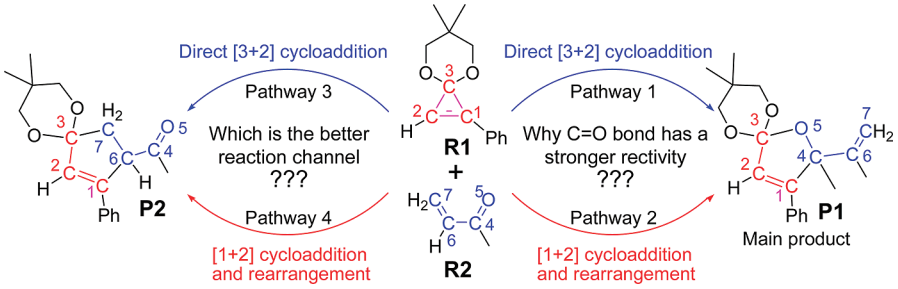

The reaction of C═O dipolarophiles with vinylcarbenes always gives [3 + 2] cycloadducts, but whether the reaction proceeds in a concerted or stepwise manner (an initial [1 + 2] cycloaddition and then a rearrangement from the [1 + 2] cycloaddition intermediate to the final [3 + 2] cycloadducts) is ambiguous. In a previous intermolecular cycloaddition reaction between C═O dipolarophiles and singlet vinylcarbenes, Boger et al. proposed that, although the [1 + 2] cycloaddition intermediate was not detected, its potential participation cannot be ruled out.[7b] Therefore, in this paper, we have considered the two possible reaction pathways and attempt to elucidate which is more favorable. The same is done for the C═C dipolarophile. The reaction of C═C dipolarophiles with singlet vinylcarbenes is somewhat different from that of C═O dipolarophiles. When a C═C dipolarophile bearing an electron-withdrawing substituent (CN^-, $COOEt^-$, etc.) tethered to it, [1 + 2] cycloadducts could be obtained. This is a stereocontrol process in favor of *cis*-cyclopropane formation, in which the electron-withdrawing substituent tethered to the C═C bond and the allylic component of the singlet vinylcarbene are in *cis*-positions.[4,7c] However, the factor responsible for this stereoselectivity remains unknown.

The C═O group is preferred to the C═C group in intermolecular cycloaddition; this can be evidenced by the detection of pure C═O [3 + 2] cycloadducts **P1** (2,8,8-trimethyl-3-phenyl-2-(eth-1-en-2-yl)-1,6,10-trioxaspiro[4.5]-dec-3-ene) in the reaction of phenyl-substituted cyclopropenone ketal (**R1**) with methyl vinyl ketone (**R2**) (Scheme 1).[7d] The C═O bond is more reactive than the C═C bond. This phenomenon is unusual and therefore needs to be investigated.

Although these kinds of 1,1/1,3-dipole cycloaddition reactions have been widely investigated in various experiments,[1,4,7] there remain many unsolved problems as described above. In the present study, we have first disclosed the reaction mechanisms theoretically shown in Scheme 1 using the B3LYP hybrid density functional method, which has been widely used in the study of organic reaction mechanisms.[9−11] Our study aims to explain the preferred chemoselectivity of C═O to C═C dipolarophiles and demonstrate the mechanisms of different reaction pathways. We also examine solvent effects to determine whether or not the polarities of the solvents have significant effects on the reaction trends.

COMPUTATIONAL DETAILS

All theoretical calculations were performed using the Gaussian 09[12] suite of programs. The geometrical structures of all the stationary points in the energy profiles were first optimized by employing the hybrid density functional B3LYP method and the 6-31G(d,p) basis set in the gas phase.[13] The Berny algorithm was employed for both minimizations and optimizations to transition states.[14] The corresponding vibrational frequencies were calculated at the same level to take into account the zero-point vibrational energy (ZPVE) and to identify whether the structure is a transition state or a minimum. We confirmed that all reactants and intermediates had no imaginary frequencies, and each transition state had only one imaginary frequency. Intrinsic reaction coordinate (IRC) calculations,[15] at the same level of theory, were performed to ensure that the transition states led to the expected reactants and products. Anharmonic frequencies[16] of the main product were calculated taking anharmonic vibrational−rotational couplings into account to compare with the experimental IR fundamentals. Solvent effects were also included at the B3LYP/6-31G(d,p) level in CH_3CN, DMF, THF, CH_2Cl_2, toluene, and benzene using the polarizable continuum model (PCM).[17] The geometrical structures of all the stationary points in the energy profiles were reoptimized. The corresponding vibrational frequencies were also calculated at the same calculation level. Thermodynamic calculations were obtained with standard statistical thermodynamics at 298.15 K and 1 atm. Moreover, the natural bond orbital (NBO) theory[18] was applied to analyze the secondary orbital interactions of representative transition states at the B3LYP/6-31G(d,p) level in the gas phase. The Gauge-independent atomic orbital (GIAO)[19]/B3LYP/aug-cc-pVDZ[20] method was employed to calculate the ^1H (in acetonitrile) and ^{13}C (in acetone) magnetic shielding constants (σ) and chemical shifts (δ) with respect to tetramethylsilane (TMS), taking solvent effects into account. Finally, to investigate the effect of basis sets, we reoptimized all of the structures based on the B3LYP/6-31G(d,p) level and calculated the vibrational frequencies at the B3LYP/6-311+G(2df,p) level of theory to ascertain whether or not the qualitative results at the B3LYP/6-31G(d,p) level are credible. We also carried out single-point energy calculations for basis sets 6-311+G(2df,p), 6-311+G(3df,2pd), and aug-cc-pVDZ based on the B3LYP/6-31G(d,p) model structures. The free energies are obtained by addition of thermal correction for Gibbs free energy at 6-31G(d,p) level to the corresponding single-point energies.

RESULTS AND DISCUSSION

1. Reaction Mechanisms. In this work, we have investigated two general reaction processes. First, the generation of the thermal π-delocalized singlet vinylcarbene (**M1** and **M2**) from cyclopropenone (**R1**) was calculated. Second, we considered four possible reaction pathways between the π-delocalized singlet vinylcarbene (**M1**) and the dipolarophile (**R2**), specifically C═O concerted (reaction pathway 1) and stepwise [3 + 2] cycloaddition (reaction pathway 2), and C═C concerted (reaction pathway 3) and stepwise [3 + 2] cycloaddition (reaction pathway 4). All compounds shown in Schemes 2 and 3 are referred to by their associated number for the sake of brevity. The corresponding representation of the free energy profile is illustrated in Figure 2. As shown in Figure 2, we set the Gibbs free energy of **R1** + **R2** as 0.0 kcal/mol as a reference in

dx.doi.org/10.1021/jo102454y |*J. Org. Chem.* 2011, 76, 3086–3095

the free energy profiles. The mechanisms of the title reaction can be illustrated as follows.

1.1. Common Reaction Process 1: Generation of Thermal π-Delocalized Singlet Vinylcarbene. All of these reactions are initiated by the generation of π-delocalized singlet vinylcarbene dipoles via opening of the three-membered ring (C1−C2−C3) in **R1**. There are two cleavage paths: one is the broken C1−C3 bond, and the other is the broken C2−C3 bond (Scheme 2). We calculated and compared the relative Gibbs free energies of the corresponding transition states and π-delocalized singlet vinylcarbene intermediates for the two cleavage modes (Figure 2). The results showed that the energy barrier for the cleavage of the C1−C3 bond via transition state **TS1** is 5.8 kcal/mol lower than that via **TS2** (27.2 versus 33.0 kcal/mol); therefore, the C1−C3 bond is more likely to break than the C2−C3 bond. Moreover, intermediate **M1** is more energetically favorable than **M2** (18.1 versus 30.1 kcal/mol). The endergonicities of formation of **M1** and **M2** suggest that the ring cleavage process for **M2** is easily reversible, and the free energy barrier for the reverse reaction is 2.9 kcal/mol. Therefore, **M1** should accumulate in higher concentrations than **M2** via the first three-membered ring breakage step, which is in accordance with experimental results that the product obtained is mainly derived from **M1**.[7d] Due to the above results, we only focused on the reaction of **M1** with **R2** through the four reaction pathways in the succeeding discussion.

Scheme 2. Generation of the 1,1/1,3-Dipole

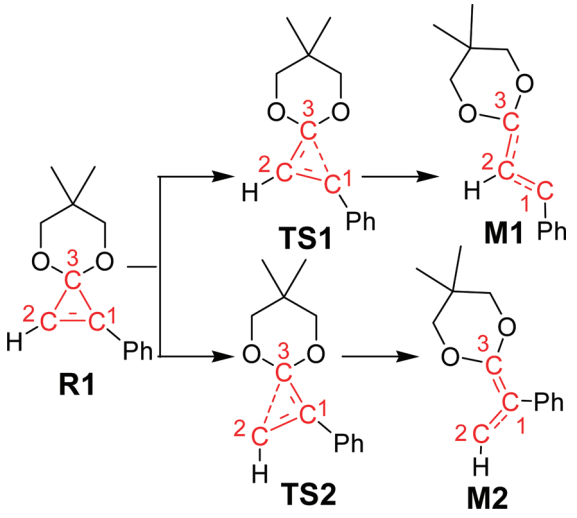

According to our investigations, we found that the greater stability of **M1** compared with **M2** is attributed to the larger number of delocalized electrons in **M1** than in **M2**. For example, the dihedral angles between the phenyl and dipole planes, which can be approximately illustrated as dihedral C2−C1−C8−C9, are smaller in **M1** (44.0°) than in **M2** (52.2°). This results in more delocalized electron distributions in **M1**. Moreover, the bond length of C1−C8 (1.452 Å) in **M1** falls between the lengths of normal C−C and C=C bonds. In **M2**, the length of the C1−C8 bond (1.503 Å) is absolutely a single bond (Figure 1). Both facts result in better degrees of electron delocalization in **M1** than in **M2**. During the three-membered ring (C1−C2−C3) opening process, only the breaking bond lengths significantly vary; the other bonds do not change much in this step. For example, the distance of C1−C3 is 1.465 Å in **R1**, 2.115 Å in **TS1**, and 2.418 Å in **M1**, but the distances of C1−C2 and C2−C3 only minimally change. This can be seen in Table 1.

*1.2. Reaction Process 2: Cycloaddition Reaction Pathways of the 1,1/1,3-Dipole (**M1**) and the C4=O5 Bond in **R2** (Reaction Pathways 1 and 2).* In reaction pathway 1, the reaction of **M1** with **R2** would directly yield the product **P1** via a five-membered ring (C1−C2−C3−C4−O5) transition state **TS1a** without any intermediate generated. In **TS1a**, the C1−C4 and C4−O5 bond distances are 2.264 and 2.493 Å, respectively, demonstrating that the [3 + 2] cycloaddition reaction takes place through asynchronous concerted mechanisms (Figure 3). The 12.2 kcal/mol Gibbs activation free energy barrier of **TS1a** indicates that the reaction could easily occur at 80 °C. The energy of product **P1** is much lower than the reactants and other stationary points in the potential energy profile (Figure 2), indicating that this reaction is an exothermic process. In addition, the Gibbs activation free energy barrier from **P1** to **TS1a** may reach up to 62.0 kcal/mol,

Scheme 3. Two Possible Reaction Pathways for C=O [3 + 2] Cycloaddition

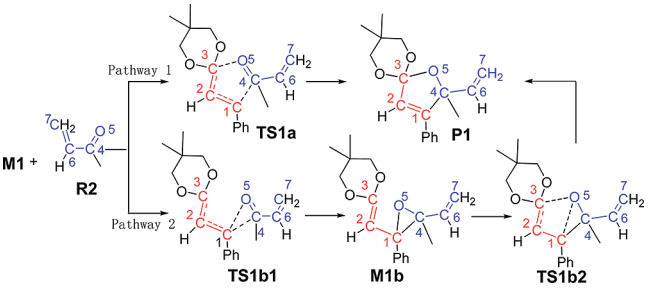

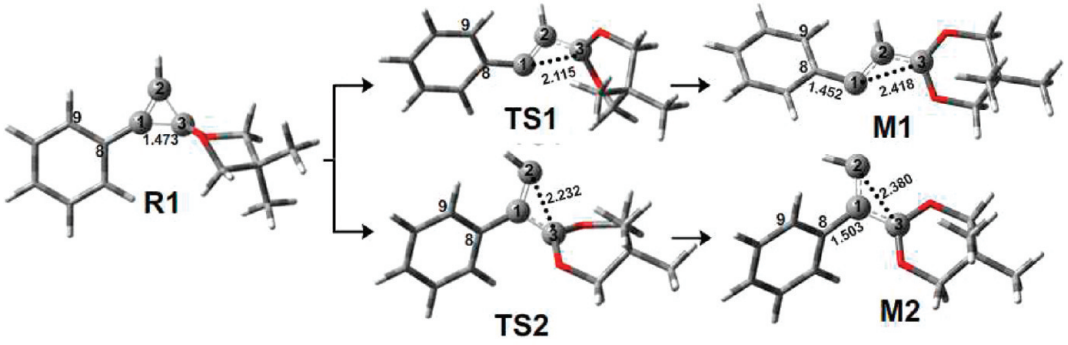

Figure 1. Optimized structures of **R1**, transition states **TS1** and **TS2**, and 1,1/1,3-dipoles **M1** and **M2**.

dx.doi.org/10.1021/jo102454y |*J. Org. Chem.* 2011, 76, 3086–3095

which is so high that the cycloaddition process is thermodynamically irreversible. The same observations can be found in reaction pathways 2, 3, and 4. Thus, the energy barrier before **P1** and **P2** is key in explaining why the concerted C═O [3 + 2] cycloaddition process is most energy-favorable.

Reaction pathway 2 consists of two steps (Scheme 3): First, **M1** undergoes [1 + 2] cycloaddition with the C4═O5 bond in **R2** to generate the three-membered ring intermediate **M1b** via the highly asynchronous concerted transition state **TS1b1**. As described in Figure 3, the C1−C4 and C1−O5 bond distances vary from 2.139 and 2.596 Å in **TS1b1** to 1.514 and 1.436 Å in **M1b**. Intermediate **M1b** then rearranges to form the [3 + 2] cycloadduct **P1** via **TS1b2**. Here, the C3−O5 bond distance shortens from 3.031 Å in **M1b** to 2.732 Å in **TS1b2** and then to 1.422 Å in **P1**. The C1−O5 bond distance elongates from 1.436 Å in **M1b** to 2.228 Å in **TS1b2** and then to 2.343 Å in **P1**. The variations in bond distances demonstrate that the C1−O5 bond is gradually broken and the C3−O5 bond is gradually formed in the rearrangement processes.

From the energy profile in Figure 2, we can see that the formation of the three-membered ring transition state **TS1b1** requires 19.2 kcal/mol of the Gibbs activation free energy, which is 7.0 kcal/mol higher than that required for **TS1a** (12.2 kcal/mol). Moreover, the Gibbs free energy barrier of the rearrangement transition state **TS1b2** is as high as 38.5 kcal/mol, suggesting that it is very difficult for the reaction to occur via this pathway to yield the product **P1** under the experimental conditions. The distance variations of some important bonds are summarized in Table 1.

*1.3. Reaction Process 2: Cycloaddition Reaction Pathways of the 1,1/1,3-Dipole (**M1**) and the C6═C7 Bond in **R2***. We first examined the concerted [3 + 2] cycloaddition reaction pathway of **M1** with the C6═C7 bond in **R2** (reaction pathway 3, Scheme 4). The only five-membered ring transition state (C1−C2−C3−C6−C7) in this reaction pathway is **TS2a**. Similar to **TS1a**, **TS2a** is also an asynchronous concerted transition state, as demonstrated by the different bond lengths of C1−C6 (2.559 Å) and C3−C7 (2.452 Å) (Figure 5). The Gibbs activation free energy barrier for this step is 22.0 kcal/mol, which is about 10 kcal/mol higher than that for reaction pathway 1.

The thermal [1 + 2] cycloaddition reaction between the C═C dipolarophile and singlet vinylcarbene is a very important reaction for the stereoselective construction of cyclopropane.[4,7c] However, the stereoselectivity of the reaction does not have a significant effect on the reaction mechanism, so we only discuss the *cis*-conformation in this paragraph. The *trans*-conformation will be discussed in detail in the succeeding sections. **M1** first goes through [1 + 2] cycloaddition with the C6═C7 bond in **R2** to generate a three-membered ring intermediate *cis*-**M2b** via the transition state *cis*-**TS2b1**. From Figure 5, this step also proceeds in a highly asynchronous concerted manner, during which the C1−C6 and C1−C7 bond distances shorten from 2.059 and 2.635 Å in *cis*-**TS2b1** to 1.550 and 1.500 Å in *cis*-**M2b**. Intermediate *cis*-**M2b** then rearranges to form the [3 + 2] cycloadduct

Table 1. Some Geometrical Parameters of Several Stationary Points along the Reaction Process (Units in Å for Bond Lengths)

SP	C1−C2	C2−C3	C1−C3	C1−O5	C1−C4	C3−O5	C4−O5
R1	1.322	1.466	1.473				
M1	1.394	1.394	2.418				
M2	1.403	2.380	1.413				
M1b	1.493	1.342	2.562	1.436	1.514	3.031	1.438
TS1	1.346	1.426	2.115				
TS2	1.378	2.232	1.428				
TS1a	1.360	1.427	2.409	2.867	2.264	2.493	1.261
TS1b1	1.400	1.390	2.479	2.596	2.139	4.269	1.256
TS1b2	1.394	1.407	2.440	2.228	1.558	2.732	1.363
P1	1.335	1.497	2.332	2.343	1.537	1.422	1.441

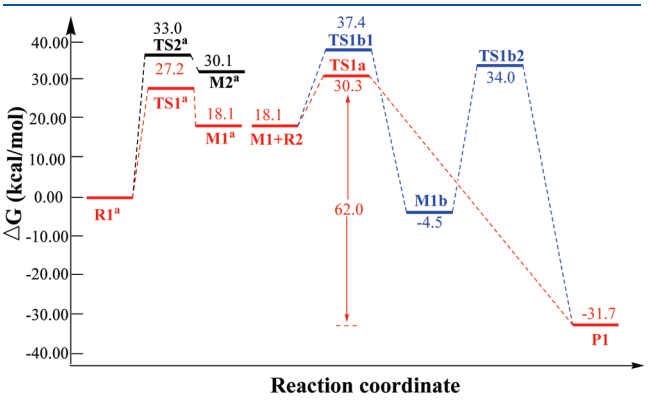

Figure 2. Gibbs free energy profiles of reaction pathways 1 and 2 (superscript "a" represents the addition of Gibbs free energy of **R2**).

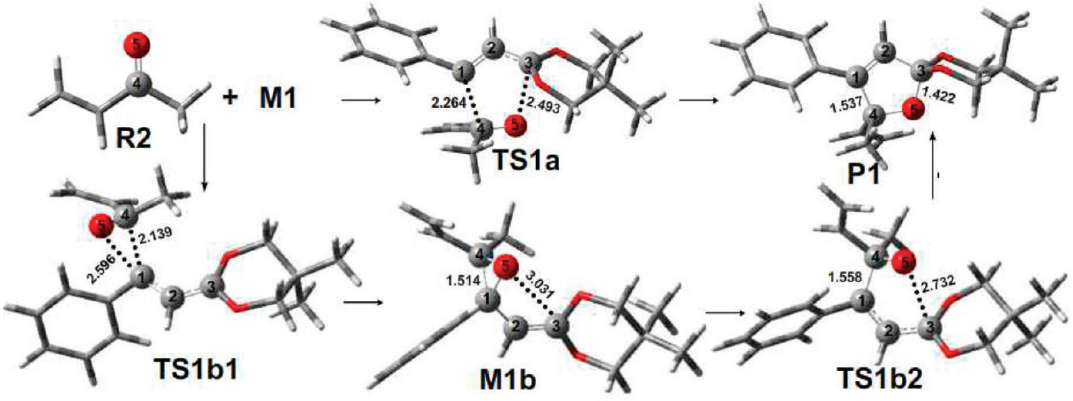

Figure 3. Structures and geometrical parameters of the stationary points in reaction pathways 1 and 2 (bond lengths in Å).

dx.doi.org/10.1021/jo102454y |*J. Org. Chem.* 2011, 76, 3086–3095

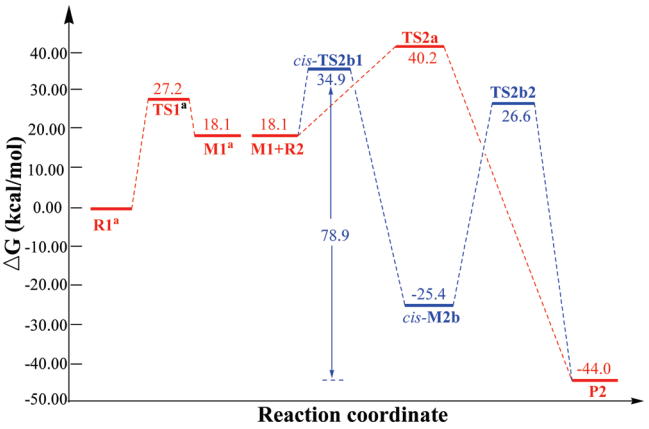

Figure 4. Energy profiles of reaction pathways 3 and 4 (superscript "a" represents the addition of Gibbs free energy of **R2**).

Scheme 4. Two Possible Reaction Pathways for C═C [3 + 2] Cycloaddition

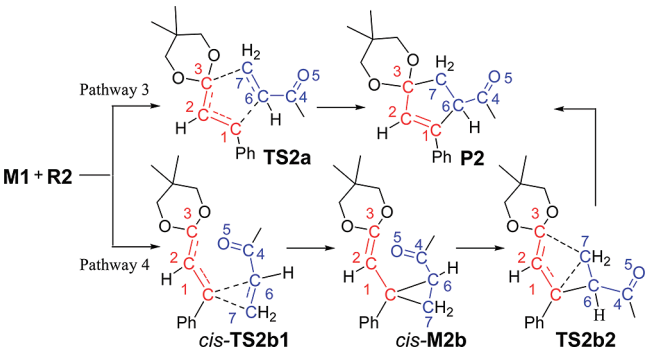

P2 via **TS2b2**, and the C3−C7 bond distance shortens from 3.674 Å in *cis*-**M2b** to 2.889 Å in **TS2b2** and then to 1.554 Å in **P2**. The C1−C7 bond distance increases from 1.500 Å in *cis*-**M2b** to 2.326 Å in **TS2b2** and then to 2.420 Å in **P2**. The bond distance variations demonstrate that the C1−C7 bond gradually breaks and the C3−C7 bond gradually forms in these rearrangement processes.

From Figure 4, we can see that the Gibbs activation free energy barrier of the first [1 + 2] cycloaddition step through transition state *cis*-**TS2b1** (16.8 kcal/mol) is 5.3 kcal/mol lower than that via **TS2a** in reaction pathway 3, but it is 4.6 kcal/mol higher than that via **TS1a** (12.2 kcal/mol, reaction pathway 1). These findings indicate that the concerted C═O [3 + 2] cycloaddition (reaction pathway 1) is the most energy-favorable one among the four possible reaction pathways.

In contrast to the preferred concerted [3 + 2] cycloaddition reaction pathway for C═O, the C═C group seems more likely to undergo the [1 + 2] cycloaddition reaction pathway than the concerted [3 + 2] cycloaddition reaction pathway, as evidenced by the lower Gibbs activation free energy barrier for **TS2a** relative to *cis*-**TS2b1** (5.3 kcal/mol). However, the Gibbs activation free energy barrier of the subsequent rearrangement from the [1 + 2] cycloadducts to the final [3 + 2] cycloadducts is so high (51.9 kcal/mol) that it is almost impossible for rearrangement to occur. This is in agreement with the intermolecular cycloaddition reaction experimental results, where the [1 + 2] cycloadducts are unable to transform to [3 + 2] cycloadducts even at 200 °C.[4]

Table 2. Some Geometrical Parameters of Several Stationary Points along the Reaction Coordinate (Units in Å for Bond Lengths)

SP	C1−C2	C2−C3	C1−C6	C1−C7	C6−C7	C7−C3	C6−C3
cis-**M2b**	1.495	1.338	1.550	1.500	1.514	3.674	3.312
TS2a	1.339	1.454	2.559	3.181	1.367	2.452	2.930
cis-**TS2b1**	1.411	1.380	2.059	2.635	1.373	4.010	3.680
TS2b2	1.395	1.398	1.503	2.326	1.505	2.889	2.867
P2	1.338	1.502	1.535	2.420	1.549	1.554	2.480

The C═C bond is more likely to undergo [1 + 2] cycloaddition rather than [3 + 2] cycloaddition. This is consistent with experimental results, where C═C [1 + 2] cycloadducts may be detected when there is an electron-withdrawing substituent group tethered to the C═C bond. However, the higher Gibbs free energy barrier of this reaction (4.6 kcal/mol) compared with concerted C═O [3 + 2] cycloaddition shows that this reaction pathway cannot predominate these four reaction pathways, explaining the main product detected. Some important bond distance variations are displayed in Table 2.

2. IR and NMR Analyses. Ab initio methods have been widely used in the determination of vibrational frequencies and NMR values to assist in the identification of experimentally observed structures.[21] In this study, theoretical IR spectra and ^{1}H and ^{13}C NMR chemical shifts were calculated to identify the geometric structure of the product through comparison with experimental spectroscopic data. Theoretical calculations always overestimate actual vibrational frequencies due to the neglect of anharmonicity.[22] As a result, many researchers apply frequency scaling factors to correct the frequencies they theoretically obtain.[21] Good overall results are usually obtained, but it is also possible that more than one scale factor exists for the same calculation method. For example, for the MP2-fu/6-31G(d) method, Hehre,[23a] Defrees,[23b] and Radom[22] gave three different scale factors. These differences can be attributed to the different molecule sets selected and various approaches adopted to determine the scale factors. To reduce these errors, and since our molecular size is not very large, we decided to calculate anharmonic frequencies taking anharmonic vibrational−rotational couplings into account using Gaussian software. In this paper, we directly calculated the anharmonic vibrational frequencies of the main product **P1** to compare with its experimental spectra. A comparison of the experimental and theoretical IR absorption vibrational frequencies of the product **P1** is displayed in Table 3. Five vibrational frequencies of 2956, 2874, 1361, 1231, and 1012 cm^{-1} obtained from experiments are assigned to the antisymmetric C−H stretching modes of CH_3 (C11 and C15), the symmetric C−H stretching modes of CH_3 (C11) and CH_2 (C2 and C4), the out-of-plane wagging vibrations of CH_2 (C2 and C4), the out-of-plane twisting vibrations of CH_2 (C2 and C4), and C−O stretching vibrations, respectively (Figure 6). The calculated harmonic and anharmonic frequencies are displayed in Table 3 to compare with the experimentally observed spectra. Our theoretically predicted harmonic frequency values significantly differ from experimentally observed IR spectra, but the anharmonic frequencies for these vibrations are in good agreement with the experimental values.

Nuclear magnetic resonance (NMR) has also proven to be a powerful method for interpreting structural information and aiding in group assignments.[24] Magnetic shielding can strongly depend on the conformation of a molecule; that is, if the molecule is flexible, multiple conformations would be considered. The product **P1** can present several conformers arising from rotations around the

dx.doi.org/10.1021/jo102454y |*J. Org. Chem.* 2011, 76, 3086–3095

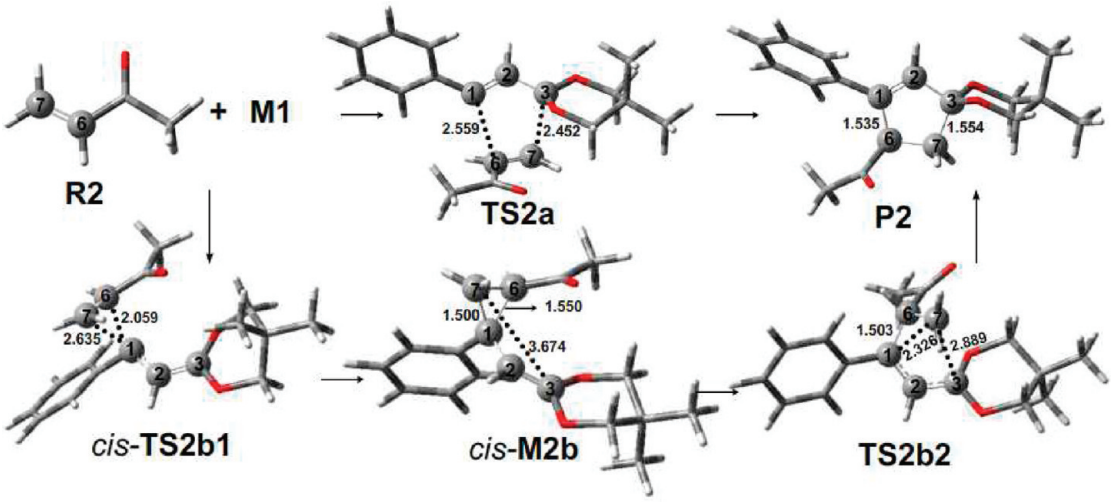

Figure 5. Structures and geometrical parameters of the stationary points in reaction pathways 3 and 4 (bond lengths in Å).

Table 3. Calculated Vibration Wave Numbers, Measured IR Band Positions (cm^{-1}), and Assignments for P1

vibrational modes	theoretical harmonicity (cm^{-1})	theoretical anharmonicity (cm^{-1})	expt (cm^{-1})
ν_{asyCH_3}	3103	2958	2956
ν_{syCH_3}	3028	2876	2874
$\nu_{CH_2\ wagging}$	1388	1362	1361
$\nu_{CH_2\ twisting}$	1258	1235	1231
ν_{C-O}	1046	1016	1012

C23−C25 single bond. In particular, we considered the following conformers: the C25−O27 and C23−C25 bonds are in either a *cis* (**P1**) or *trans* (**P1′**) relationship (Figure 6). **P1** is only 0.5 kcal/mol lower than **P1′**, and they can transform into each other. In the following sections, we compare their NMR values.

Given all of the ab initio methods employed in predicting chemical shifts, the B3LYP method is known to perform well and be computationally inexpensive.[24] Larger basis sets are needed to obtain accurate magnetic shielding values.[25] In this study, NMR chemical shifts (δ) were evaluated using the B3LYP/aug-cc-pVDZ method, as recommended by Rablen.[26] Solvent effects were also accounted for (in the experiment, ^{1}H NMR results are recorded in acetone-d_6 with a frequency of 600 MHz and ^{13}C NMR results are recorded in CD_3CN with a frequency of 150 MHz) to compare with experimental results. To eliminate systematic errors, the NMR chemical shifts (δ_A, A = ^{1}H or ^{13}C) were calculated as the differences of isotropic shielding constants (σ) with respect to the TMS reference ($\delta_A = \sigma_{TMS} - \sigma_A$). From Table 4, we can see that the calculated chemical shielding values for **P1** and **P1′** are very similar. Although their values do not agree very well with the experimental results in an absolute numerical sense, the linear regressions are characterized by large correlation coefficients of 0.98 for ^{1}H and ^{13}C for both **P1** and **P1′**.

As described above, our calculated IR and NMR values are in good agreement with experimental IR spectra and NMR results for the optimized structures of **P1** and **P1′**, indicating that we obtained the correct geometric structure of the product.

3. Why Is the C═O Bond More Reactive Than the C═C Bond in R2? To explain why C═O is more reactive than the C═C

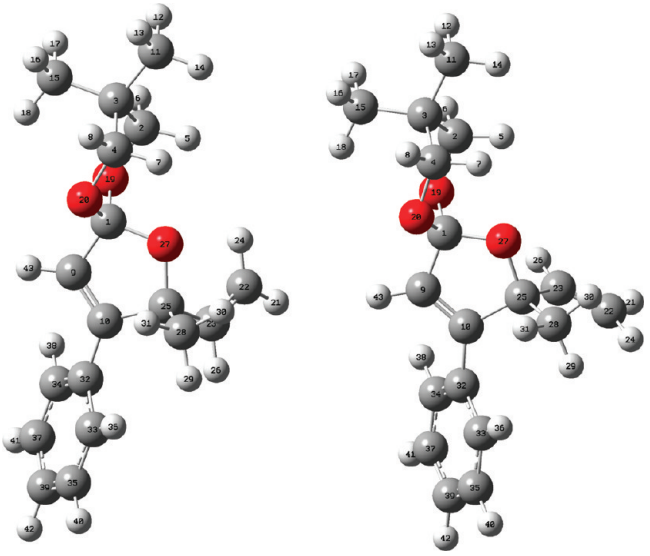

Figure 6. Optimized structures of **P1** and **P1′** at the B3LYP/6-31G (d,p) level.

dipolarophile when they coexist, we performed a second-order perturbation analysis of the NBOs on transition states **TS1a** and **TS2a**. NBO analysis could help evaluate intramolecular interactions. For each (i) donor and (j) acceptor, the second-order perturbation interaction energy can be expressed by the equation[18a]

$$E(2) = E_{ij} = q_i F_{ij}^2 / \varepsilon_i \varepsilon_j$$

where F_{ij} is the off-diagonal element in the NBO Fock matrix, q_i is the donor orbital occupancy, and ε_i and ε_j are diagonal elements (orbital energies).

NBO analysis for **TS1a** (the most energy-favorable transition state) reveals that two considerable interactions contribute to the stabilization of **TS1a**: the first corresponding to the charge transfer from the n of the negative center C1 atom to the n* of the positive center C4 atom (stabilization by 131.2 kcal/mol), and the second corresponding to the n of the negative center O5 atom feedback to the n* of the positive center C3 atom (40.9 kcal/mol). For **TS2a**, the two considerable interactions between

dx.doi.org/10.1021/jo102454y |J. Org. Chem. 2011, 76, 3086–3095

Table 4. Comparison of Theoretical (PCM/B3LYP/aug-cc-pVDZ) ^{1}H and ^{13}C NMR Chemical Shifts, with Experimental Results for the Atoms in the Products P1 and P1′ (units of ppm)

^{1}H	theoretical **P1**	theoretical **P1′**	expt (ppm)	^{13}C	theoretical **P1**	theoretial **P1′**	expt (ppm)
H5	4.47	4.35	4.15	C1	122.1	121.5	113.3
H7	4.38	4.31		C2	72.4	72.0	71.6
H6	3.63	3.60	3.45	C3	40	38.9	29.9
H8	3.60	3.57		C4	71.7	71.6	71.5
H12	0.97	0.94	0.81	C9	124.2	126.7	116.4
H13	0.97	0.93		C10	158.4	156.8	142.2
H14	0.89	0.78		C11	20.8	21.3	22.2
H16	0.86	0.86	1.31	C15	21.1	21.5	23.6
H17	0.87	0.87		C22	110.2	112.3	116.4
H18	2.23	2.28		C23	144.3	145.6	137.4
H21	5.33	5.21	5.04	C25	95.7	95.3	87.2
H24	5.87	5.28	5.33	C28	29.7	23.3	26.2
H26	6.26	6.28	6.00	C32	137.4	137.7	135.0
H29	2.18	2.28	1.47	C33	126.1	127.1	121.5
H30	1.68	1.69		C34	129.8	130.4	133.0
H31	1.77	1.62		C35	126.6	126.3	129.0
H36	8.01	7.83	7.81	C37	128.1	127.5	129.1
H38	7.60	7.55		C39	127.5	127.4	127.9
H40	7.87	7.82	7.34				
H41	7.75	7.73					
H42	7.81	7.75	7.29				
H43	5.73	5.90	6.50				

Table 5. Second-Perturbation Energies $E(2)$ (kcal/mol) of Donor−acceptor Interactions with Respect to TS1a and TS2a

TS	donor	acceptor	interaction	$E(2)$
TS1a	LP(1)C1	LP*(1)C4	n−n*	131.2
	LP(3)O5	LP*(1)C3	n−n*	40.9
	BD(2)C1−C2	LP*(1)C4	π−n*	4.1
	LP*(1)C4	BD*(2)C1−C8	n*−π*	3.1
	LP(1)O5	LP*(1)C3	n−n*	2.7
TS2a	BD*(2)C1−C8	BD*(2)C6−C7	π*−π*	25.5
	BD(2)C6−C7	LP*(1)C3	π−n*	35.5
	BD*(2)C6−C7	BD*(2)C1−C2	π*−π*	7.2
	BD(2)C1−C2	BD*(2)C6−C7	π−π*	2.1
	BD(2)C1−C8	BD*(2)C6−C7	π−π*	6.2
	LP*(1)C3	BD*(2)C6−C7	n*−π*	8.5
	BD(1)C7−H8	LP*(1)C3	π−n*	2.4

M1 and **R2**, specifically those of π* of the C1−C8 bond interacting with π* of the C6−C7 bond (25.5 kcal/mol) and π of the C6−C7 bond interacting with n* of the C3 atom (35.5 kcal/mol), are rather weak relative to those of **TS1a** (Table 5).

In addition, when we analyzed the NBO charge distributions (Table 6), we found that **TS1a** can be described as a zwitterionic transition state formed by the interaction of the negatively charged center C1 atom with the positively charged center C4 atom and the positively charged center C3 atom with the negatively charged center O5 atom. The two strong interactions may explain the two strong second-order perturbation interactions in **TS1a** and its lowest Gibbs activation free energy barrier in all the transition states. In **TS2a**, there is only one

Table 6. NBO Charges on C1, C2, C3, C4, O5, C6, and C7 Atoms in R2, M1, TS1a, and TS2a at the B3LYP/6-31G (d, p) Level (units of e)

	C1	C2	C3	C4	O5	C6	C7
R2				0.546	−0.545	−0.345	−0.336
M1	−0.067	−0.478	0.775				
TS1a	−0.029	−0.447	0.869	0.476	−0.731	−0.294	−0.405
TS2a	−0.017	−0.440	0.759	0.550	−0.593	−0.290	−0.514

advantageous interaction between the positive charge center on the C3 atom and the negative charge center on the C7 atom. The interaction between atoms C1 and C6 is disadvantageous because their NBO charges are both negative, resulting in a longer C1−C6 bond length (2.559 Å) in **TS2a**. In summary, the charge transfer from the C1 atom to the C4 atom and the electron feedback from the O5 atom to the C3 atom cause **TS1a** to have the lowest Gibbs activation free energy barrier.

4. Stereoselectivity of the Thermal [1 + 2] Cycloaddition Reaction between the C═C Dipolarophile and Vinylcarbene. We have discussed the four possible reaction pathways of the title reaction and the preferred chemoselectivity of the C═O dipolarophile rather than the C═C dipolarophile in the thermal [3 + 2] cycloaddition reaction. Another intriguing experimental result was observed when the C═C dipolarophile bearing an electron-withdrawing substituent was allowed to react with the singlet vinylcarbene. This reaction preferably yielded *cis*-cyclopropanes.[4,7c] Thus, it would be meaningful to determine the stereocontrol factor. In fact, the reaction of **M1** with the C6═C7 bond in **R2** can lead to the two intermediates *cis*-**M2b** and *trans*-**M2b** through the transition states *cis*-**TS2b1** and *trans*-**TS2b1**, respectively (Figure 7). The computed Gibbs activation free

dx.doi.org/10.1021/jo102454y |J. Org. Chem. 2011, 76, 3086–3095

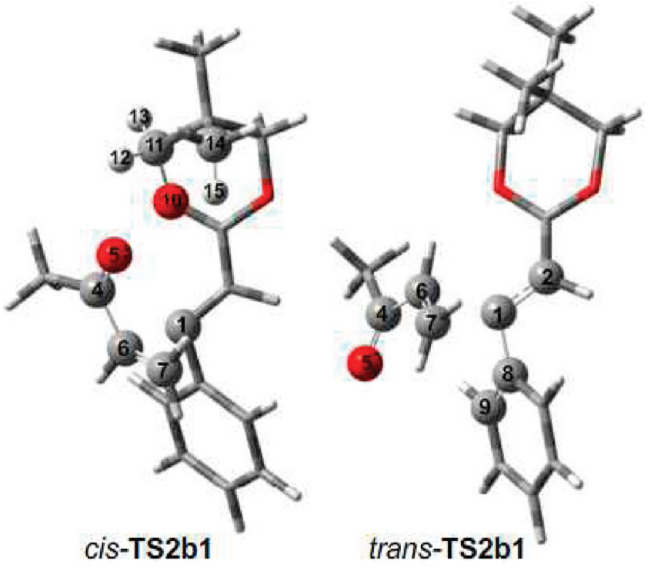

Figure 7. Optimized structures of *cis*-**TS2b1** and *trans*-**TS2b1**.

Table 7. Second-Perturbation Energy $E(2)$ (kcal/mol) of Donor−acceptor Interactions with Respect to C4═O5 in *cis*-TS2b1 and *trans*-TS2b1

TS	donor	acceptor	interaction	$E(2)$
cis-**TS2b1**	LP(1)O5	BD*(1)C11−H12	n−σ^*	0.55
	LP(1)O5	BD*(1)C14−H15	n−σ^*	0.21
	LP(2)O5	BD*(1)C11−H12	n−σ^*	1.04
	LP(1)O10	BD*(2)C4−O5	n−π^*	0.29
	LP(1)C1	BD*(2)C4−O5	n−π^*	2.01
trans-**TS2b1**	BD(2)C4−O5	BD*(1)C1−C2	$\pi-\sigma^*$	0.14
	BD(2)C4−O5	BD*(1)C8−C9	$\pi-\pi^*$	0.07
	BD*(2)C4−O5	BD*(1)C1−C2	$\pi^*-\sigma^*$	0.08
	BD(2)C8−C9	BD*(1)C4−O5	$\pi-\sigma^*$	0.06

energy barrier for *cis*-**TS2b1** (16.8 kcal/mol) is 0.9 kcal/mol lower than that for *trans*-**TS2b1** (17.7 kcal/mol). Assuming that the ratio of reaction rate constants for the [1 + 2] cycloaddition reaction is determined by the difference in activation free energies, the k(*cis*-**M2b**)/k(*trans*-**M2b**) ratio at 298.15 K is 4.6. This ratio could explain why the *cis*-stereoisomer was always determined to be the major product of the reaction. To analyze which factor is responsible for this stereocontrol, NBO analysis was performed for the transition states. The results are shown in Table 7. For *cis*-**TS2b1**, the second-order energies associated with the donation of one lone-pair from O in C4═O5 to the σ^*(C11−H12) and σ^*(C14−H15) acceptors are calculated to be 0.55 and 0.21 kcal/mol, respectively. The donation of another lone-pair from O in C4═O5 to the σ^*(C11−H12) acceptor results in a stabilization energy of 1.04 kcal/mol. Similarly, the donation of a lone-pair from O10 and C1 to the π^* (C4═O5) acceptor are 0.29 and 2.01 kcal/mol, respectively. For *trans*-**TS2b1**, only a few rather small second-order interactions are found (Table 7). Thus, it can be concluded that the *cis*-stereocontrol phenomenon originates from advantageous second-order interactions between the electron-withdrawing substituent tethered to the C═C bond and the allylic component of the singlet vinylcarbene.

Table 8. ΔG at the B3LYP/6-31G (d, p) Level in the Solvents CH_3CN, DMF, THF, CH_2Cl_2, Toluene, and Benzene Using the PCM Model (units of kcal/mol)

ΔG	gas phase	CH_3CN	DMF	THF	CH_2Cl_2	toluene	benzene
$\Delta G_{\text{TS1-R1}}$	27.2	23.5	23.5	26.9	27.1	25.5	25.6
$\Delta G_{\text{TS1a-(M1+R2)}}$	12.2	18.9	18.8	17.5	17.6	14.9	14.8
$\Delta G_{\text{TS1b1-(M1+R2)}}$	19.2	20.2	20.1	20.3	20.3	19.9	19.8
$\Delta G_{\text{TS1b2-M1b}}$	38.5	32.3	32.2	38.8	39.1	36.3	36.4
$\Delta G_{\text{TS2-R1}}$	33.0	26.6	26.6	31.5	31.7	30.0	30.2
$\Delta G_{\text{TS2a-(M1+R2)}}$	22.0	29.1	29.1	27.9	28.1	25.3	25.2
$\Delta G_{\text{cis-TS2b1-(M1+R2)}}$	16.8	24.9	24.9	23.3	23.5	20.3	20.2
$\Delta G_{\text{TS2b2-cis-M2b}}$	51.9	51.9	51.9	54.3	54.6	51.9	51.9

5. Solvent Effect. The geometrical structures of all stationary points in the energy profiles were optimized, and the corresponding vibrational frequencies were calculated by employing the hybrid density functional B3LYP method with 6-31G(d,p) basis set in six solvents with different polarities, namely, CH_3CN, DMF, THF, CH_2Cl_2, toluene, and benzene. The PCM model was used here. The ΔG values obtained in the six solvents are summarized in Table 8. As can been seen from the table, although several significant changes for various ΔG values in the different solvents are found, the reaction trends and the main product in the different solvents do not vary. All of the $\Delta G_{\text{TS1-R1}}$ values remain lower than the $\Delta G_{\text{TS2-R1}}$ values; all the $\Delta G_{\text{TS1a-(M1+R2)}}$ values (reaction pathway 1) are lower than the $\Delta G_{\text{TS1b1-(M1+R2)}}$ (reaction pathway 2), $\Delta G_{\text{TS2a-(M1+R2)}}$ (reaction pathway 3), or $\Delta G_{\text{cis-TS2b1-(M1+R2)}}$ values (reaction pathway 4). These results are in agreement with the conclusions obtained under the gas-phase condition, in which **M1** is always more easily obtained than **M2** and the concerted C═O [3 + 2] cycloaddition reaction pathway always predominates over the other possible reaction pathways.

6. Effect of Basis Sets. To further examine basis set effects, we reoptimized all of the structures in the energy profile and calculated the frequencies for a larger basis set, B3LYP/6-311+G(2df,p). The optimized structures at the two levels do not significantly vary. However, the relative free energies have significant errors. Comparing the free energy barriers at the two levels, we found that the error between the two calculation levels ranges from 1.1 to 5.6 kcal/mol. We also tried another method to obtain the free energies at 6-311+G(2df,p) level by adding the thermal correction for Gibbs free energy at 6-31G(d,p) level to the corresponding single-point energies at 6-311+G(2df,p) level. From Table 9, we can see that the free energy barriers using this method are very similar with that obtained directly by calculating the frequencies. Therefore, we calculated the free energies at 6-311++G(3df,2dp) and aug-cc-pVDZ levels using this method in order to save computing resource. The corresponding Gibbs free energies of all the structures in the energy profiles are listed in Tables S3 and S4 in the Supporting Information. As can be seen from Table 9, the comparison between values obtained at different levels of basis sets shows that larger basis sets result in similar activation free energy barriers. The Gibbs free energy barriers at the aug-cc-pVDZ level are largely similar to those at the B3LYP/6-31G(d,p) level. It is difficult to determine which basis set gives more accurate free energy barriers. Fortunately, the trend of the four reaction pathways does not change with the different basis sets. No matter which basis set is chosen, the concerted C═O [3 + 2] cycloaddition reaction is always the most energy-favorable one among the four reaction pathways. The C═C dipolarophile is also more likely to undergo [1 + 2], rather than [3 + 2], cycloaddition.

dx.doi.org/10.1021/jo102454y |*J. Org. Chem.* 2011, 76, 3086–3095

Table 9. Gibbs Activation Free Energy Barriers for Different Basis Sets (Values in Parentheses Are Free Energy Barriers Obtained by Calculating the Frequencies)

ΔG	6-31G(d,p)	6-311+G(2df,p)	6-311+G(3df,2pd)	aug-cc-pVDZ
$\Delta G_{TS1\text{-}R1}$	27.3	25.4(25.4)	25.0	25.4
$\Delta G_{TS1a\text{-}(M1+R2)}$	12.2	16.9(16.7)	17.0	15.6
$\Delta G_{TS1b1\text{-}(M1+R2)}$	19.2	24.0(23.8)	24.2	22.3
$\Delta G_{TS1b2\text{-}M1b}$	38.5	36.4(35.4)	36.6	35.5
$\Delta G_{TS2\text{-}R1}$	33.0	30.8(30.2)	30.5	29.6
$\Delta G_{TS2a\text{-}(M1+R2)}$	22.0	26.6(26.4)	26.7	25.0
$\Delta G_{cis\text{-}TS2b1\text{-}(M1+R2)}$	16.8	22.7(22.4)	22.9	20.6
$\Delta G_{TS2b2\text{-}cis\text{-}M2b}$	51.9	50.7(50.8)	50.7	50.1

Therefore, our analyses based on the results at the 6-31G(d,p) level are credible.

CONCLUSIONS

In this article, the integrated mechanism of the title reaction was investigated using the density functional theory (DFT). The good overall agreement between the experimental and theoretical IR spectra and ^{1}H and ^{13}C chemical shifts for the obtained product demonstrates that we obtained the correct geometric structures of the product for the title reaction. The calculated results revealed that, under experimental conditions (80 °C), the reaction takes place via two steps: Initially, the three-membered ring (C1−C2−C3) in **R1** opens to form intermediate 1,1/1,3-dipolar π-delocalized singlet vinylcarbenes **M1** and **M2**. The endergonic characteristics of this step and the instability of **M2** relative to **M1** indicate that **M1** is the main cleavage intermediate. The 1,1/1,3-dipole **M1** then undergoes [3 + 2] cycloaddition with **R2**. There are four possible cycloaddition reaction pathways between **M1** and C═O and C═C dipolarophiles in **R2**. The Gibbs free energy barrier for the concerted [3 + 2] cycloaddition reaction of C═O dipolarophiles with singlet vinylcarbenes **M1** is the lowest among the four possible reaction pathways, suggesting that reaction pathway 1 is the most competitive. This can explain why the C═O [3 + 2] cycloadduct is the main product in the experiment. The C═C dipolarophile is more likely to undergo [1 + 2] cycloaddition rather than concerted [3 + 2] cycloaddition, which is very interesting and highly unusual.

NBO second-order perturbation and NBO charge analyses indicate that charge transfers and electron feedback cause **TS1a** to have a low Gibbs activation free energy barrier. The *cis*-stereocontrol phenomenon of thermal [1 + 2] cycloaddition between C═C dipolarophiles and vinylcarbenes originates from advantageous second-order interactions between the electron-withdrawing substituent tethered to the C═C bond and the allylic component of the singlet vinylcarbene. Further solvent effect considerations show that the polarities of the reaction solvents have little impact on the reaction trends and processes.

Finally, a comparison of the results for different basis sets reveals that, although there are some errors between the calculated energies, the findings based on the B3LYP/6-31G(d,p) level are reliable.

ASSOCIATED CONTENT

Supporting Information. Cartesian coordinates and the ZPE (zero-point energies), E (electronic energies), E' (sum of electronic and zero-point energies), H (sum of electronic and thermal enthalpies), and G (sum of electronic and thermal free energies) of the reactants, intermediates, transition states, and products obtained at the B3LYP/6-31G(d,p) level. The Gibbs free energies of all reported structures for basis sets 6-311+G-(2df,p), 6-311++G(3df,2pd), and aug-cc-pVDZ. The Gibbs free energies of all stationary points computed in the solvents CH_3CN, DMF, THF, CH_2Cl_2, toluene, and benzene using the PCM model. This material is available free of charge via the Internet at http://pubs.acs.org.

AUTHOR INFORMATION

Corresponding Author

*Address correspondence to tschu008@163.com.

ACKNOWLEDGMENT

This work was supported by the National Natural Science Foundation of China (Grant No. 10874096).

REFERENCES

(1) Boger, D. L.; Brotherton, C. E. *J. Am. Chem. Soc.* **1984**, *106*, 805.
(2) Rolf, H. *Angew. Chem., Int. Ed. Engl.* **1963**, *2*, 565.
(3) *1,3-Dipolar Cycloaddition Chemistry*; Padwa, A., Ed.; Wiley: New York, 1984; Vols. 1, 2.
(4) Boger, D. L.; Brotherton, C. E. *J. Am. Chem. Soc.* **1986**, *108*, 6695.
(5) (a) Trost, B. M.; Cramer, N.; Silverman, S. M. *J. Am. Chem. Soc.* **2007**, *129*, 12396. (b) Trost, B. M.; Silverman, S. M.; Stambuli, J. P. *J. Am. Chem. Soc.* **2007**, *129*, 12398. (c) Trost, B. M.; Silverman, S. M. *J. Am. Chem. Soc.* **2010**, *132*, 8238.
(6) (a) Xu, Z. R.; Lu, X. Y. *Tetrahedron Lett.* **1997**, *38*, 3461. (b) Xu, Z. R.; Lu, X. Y. *J. Org. Chem.* **1998**, *63*, 5031. (c) Xu, Z. R.; Lu, X. Y. *Tetrahedron Lett.* **1999**, *40*, 549.
(7) (a) Boger, D. L.; Brotherton, C. E. *Tetrahedron Lett.* **1984**, *25*, 5611. (b) Boger, D. L.; Brotherton, C. E.; Georg, G. I. *Tetrahedron Lett.* **1984**, *25*, 5615. (c) Boger, D. L.; Wysocki, R. J. *J. Org. Chem.* **1988**, *53*, 3408. (d) Patel, P. R.; Boger, D. L. *J. Am. Chem. Soc.* **2010**, *132*, 8527.
(8) (a) Iwasawa, N.; Shido, M.; Kusama, H. *J. Am. Chem. Soc.* **2001**, *123*, 5814. (b) Kusama, H.; Funami, H.; Takaya, J.; Iwasawa, N. *Org. Lett.* **2004**, *6*, 605. (c) Kusama, H.; Funami, H.; Shido, M.; Hara, Y.; Takaya, J.; Iwasawa, N. *J. Am. Chem. Soc.* **2005**, *127*, 2709.
(9) (a) Li, J.; Jiang, W. Y.; Han, K. L.; He, G. Z.; Li, C. *J. Org. Chem.* **2003**, *68*, 8786. (b) Zhao, G. J; Liu, J.-Y.; Zhou, L. C.; Han, K. L. *J. Phys. Chem. B* **2007**, *111*, 8940. (c) Wang, H. M.; Wang, Y.; Han, K. L.; Peng, X. J. *J. Org. Chem.* **2005**, *70*, 4910. (d) Chen, X. F.; Hou, C. Y.; Han, K. L. *J. Phys. Chem. A* **2010**, *114*, 1169. (e) Zhao, G. J.; Han, K. L. *Biophys. J.* **2008**, *94*, 38. (f) Han, K. L.; He, G. Z. *J. Photochem. Photobiol., C* **2007**, *8*, 55.
(10) (a) Palacios, F.; Herran, E.; Alonso, C.; Rubiales, G.; Lecea, B.; Ayerbe, M.; Cossio, F. P. *J. Org. Chem.* **2006**, *71*, 6020. (b) Cossio, F. P.; Alonso, C.; Lecea, B.; Ayerbe, M.; Rubiales, G.; Palacios, F. *J. Org. Chem.*

2006, *71*, 2839. (c) Arrieta, A.; Otaegui, D.; Zubia, A.; Cossio, F. P.; de la Hoz, A.; Herrero, M. A.; Prieto, P.; Foces-Foces, C.; Pizarro, J. L.; Arriortua, M. *J. Org. Chem.* **2007**, *72*, 4313. (d) Aginagalde, M.; Bello, T.; Masdeu, C.; Vara, Y.; Arrieta, A.; Cossio, F. P. *J. Org. Chem.* **2010**, *75*, 7435. (e) Aginagalde, M.; Vara, Y.; Arrieta, A.; Zangi, R.; Cebolla, V. L.; Delgado-Camon, A.; Cossio, F. P. *J. Org. Chem.* **2010**, *75*, 2776.

(11) (a) Garcia-Exposito, E; Bearpark, M. J.; Ortuno, R. M.; Robb, M. A.; Branchadell, V. *J. Org. Chem.* **2002**, *67*, 6070. (b) Torrente, S.; Noya, B.; Branchadell, V.; Alonso, R. *J. Org. Chem.* **2003**, *68*, 4772. (c) Illa, O.; Bagan, X.; Cazorla, A. M.; Lyon, C.; Baceiredo, A.; Branchadell, V.; Ortuno, R. M. *J. Org. Chem.* **2006**, *71*, 5320. (d) Lecea, B.; Ayerbe, M.; Arrieta, A.; Cossio, F. P.; Branchadell, V.; Ortuno, R. M.; Baceiredo, A. *J. Org. Chem.* **2007**, *72*, 357.

(12) Frisch, M. J.; Trucks, G. W.; Schlegel, H. B.; Scuseria, G. E.; Robb, M. A.; Cheeseman, J. R.; Scalmani, G.; Barone, V.; Mennucci, B.; Petersson, G. A.; Nakatsuji, H.; Caricato, M.; Li, X.; Hratchian, H. P.; Izmaylov, A. F.; Bloino, J.; Zheng, G.; Sonnenberg, J. L.; Hada, M.; Ehara, M.; Toyota, K.; Fukuda, R.; Hasegawa, J.; Ishida, M.; Nakajima, T.; Honda, Y.; Kitao, O.; Nakai, H.; Vreven, T.; Montgomery, J. A.; Jr.; Peralta, J. E.; Ogliaro, F.; Bearpark, M.; Heyd, J. J.; Brothers, E.; Kudin, K. N.; Staroverov, V. N.; Kobayashi, R.; Normand, J.; Raghavachari, K.; Rendell, A.; Burant, J. C.; Iyengar, S. S.; Tomasi, J.; Cossi, M.; Rega, N.; Millam, J. M.; Klene, M.; Knox, J. E.; Cross, J. B.; Bakken, V.; Adamo, C.; Jaramillo, J.; Gomperts, R.; Stratmann, R. E.; Yazyev, O.; Austin, A. J.; Cammi, R.; Pomelli, C.; Ochterski, J. W.; Martin, R. L.; Morokuma, K.; Zakrzewski, V. G.; Voth, G. A.; Salvador, P.; Dannenberg, J. J.; Dapprich, S.; Daniels, A. D.; Farkas, O.; Foresman, J. B.; Ortiz, J. V.; Cioslowski, J. Fox, D. J. *Gaussian 09*, revision A.02; Gaussian, Inc.: Wallingford, CT, 2009.

(13) (a) Becke, A. D. *J. Chem. Phys.* **1993**, *98*, 5648. (b) Lee, C. T.; Yang, W. T.; Parr, R. G. *Phys. Rev. B* **1988**, *37*, 785.

(14) Li, X.; Frisch, M. J. *J. Chem. Theory Comput.* **2006**, *2*, 835.

(15) (a) Gonzalez, C.; Schlegel, H. B. *J. Chem. Phys.* **1989**, *90*, 2154. (b) Gonzalez, C.; Schlegel, H. B. *J. Phys. Chem.* **1990**, *94*, 5523.

(16) (a) Barone, V.; Cossi, M.; Rega, N.; Scalmani, G. *J. Comput. Chem.* **2003**, *24*, 669. (b) Barone, V. *J. Chem. Phys.* **2005**, *122*, 1.

(17) (a) Barone, V.; Cossi, M. *J. Phys. Chem. A* **1998**, *102*, 1995. (b) Mennucci, B.; Tomasi, J. *J. Chem. Phys.* **1997**, *106*, 5151.

(18) (a) Reed, A. E.; Weinstock, R. B.; Weinhold, F. *J. Chem. Phys.* **1985**, *83*, 735. (b) Carpenter, J. E.; Weinhold, F. *THEOCHEM* **1988**, *169*, 41. (c) Reed, A. E.; Curtiss, L. A.; Weinhold, F. *Chem. Rev.* **1988**, *88*, 899. (d) Ito, K.; Hara, Y.; Mori, S.; Kusama, H.; Iwasawa, N. *Chem.—Eur. J.* **2009**, *15*, 12408.

(19) (a) Ditchfie., R *J. Chem. Phys.* **1972**, *56*, 5688. (b) Wolinski, K.; Hinton, J. F.; Pulay, P. *J. Am. Chem. Soc.* **1990**, *112*, 8251.

(20) (a) Dunning, T. H., Jr. *J. Chem. Phys.* **1989**, *90*, 1007. (b) Kendall, R. A.; Dunning, T. H.; Harrison, R. J. *J. Chem. Phys.* **1992**, *96*, 6796–6806.

(21) (a) Subashchandrabose, S.; Krishnan, A. R.; Saleem, H.; Thanikachalam, V.; Manikandan, G.; Erdogdu, Y. *J. Mol. Struct.* **2010**, *981*, 59. (b) Prestianni, A.; Joubert, L.; Chagnes, A.; Cote, G.; Ohnet, M. N.; Rabbe, C.; Charbonnel, M. C.; Adamo, C. *J. Phys. Chem. A* **2010**, *114*, 10878. (c) Ayyappan, S.; Sundaraganesan, N.; Aroulmoji, V.; Murano, E.; Sebastian, S. *Spectrochim. Acta, Part A* **2010**, *77*, 264. (d) Botek, E.; d'Antuono, P.; Jacques, A.; Carion, R.; Champagne, B.; Maton, L.; Taziaux, D.; Habib-Jiwan, J.-L. *Phys. Chem. Chem. Phys.* **2010**, *12*, 14172.

(22) Scott, A. P.; Radom, L. *J. Phys. Chem.* **1996**, *100*, 16502.

(23) (a) Hout, R. F.; Levi, B. A.; Hehre, W. J. *J. Comput. Chem.* **1982**, *3*, 234. (b) DeFrees, D. J.; McLean, A. D. *J. Chem. Phys.* **1985**, *82*, 333.

(24) Jain, R.; Bally, T.; Rablen, P. R. *J. Org. Chem.* **2009**, *74*, 4017.

(25) (a) Kupka, T.; Ruscic, B.; Botto, R. E. *J. Phys. Chem. A* **2002**, *106*, 10396. (b) Magyarfalvi, G.; Pulay, P. *J. Chem. Phys.* **2003**, *119*, 1350.

(26) Jain, R.; Bally, T.; Rablen, P. R. *J. Org. Chem.* **2009**, *74*, 4017.